CrystEngComm

PAPER

View Article Online
View Journal | View Issue

Cite this: *CrystEngComm*, 2017, **19**, 528

One-pot hydrothermal synthesis of ZnC_4O_4 concave microspheres with superhydrophobic and superoleophilic properties†

Wen Meng,[a] Lahong Zhang,[a] Feng Li,*[a] Taohai Li[a] and Wei Cao[b]

Received 8th October 2016,
Accepted 10th December 2016

DOI: 10.1039/c6ce02144a

www.rsc.org/crystengcomm

In this study, we report a facile solution route to prepare superhydrophobic and superoleophilic ZnC_4O_4 concave microspheres. The surface morphologies and chemical compositions were determined through scanning electron microscopy (SEM), transmission electron microscopy (TEM), energy dispersive X-ray spectroscopy (EDX), X-ray powder diffraction (XRD), and X-ray photoelectron spectroscopy (XPS). The wettability of the as-synthesized ZnC_4O_4 coordination compound surface was studied by measuring the contact angle (CA). A static CA for water over 160° was observed, which was closely related to both the structure and chemical modification of ZnC_4O_4, and a 0° static CA for octane was observed, which showed that the as-prepared ZnC_4O_4 surface had superoleophilic properties. Furthermore, the as-prepared ZnC_4O_4 surface showed superhydrophobicity for some corrosive liquids, such as acidic and basic aqueous solutions.

Introduction

Inspired by the self-cleaning lotus' leaf and "anti-water" feather's water sliding, the phenomenon defined as "superhydrophobicity" can be visualized as a drop of liquid sitting on a surface forming a large contact angle (CA), typically greater than 150 degrees for pure water and easily rolling on or sliding off the surface. The lotus leaf[1] and skin on gecko's hierarchical foot[2] have an ultrahigh CA, but ultralow water adhesion, representing ideal super-hydrophobic surfaces. Water droplets on such surfaces can easily roll off to remove loosely adhered dirt particles and debris from the surfaces if the substrate is slightly tilted (extremely small roll-off tilt angles <10°). Within the fraction of interaction between the surface and droplet, the actual per unit planar area is represented as the roughness, which is an important geometric factor for the hydrophobic property. The reduction in contact area can change the contact to a Cassie state, as determined by the Cassie–Baxter equation.[3–7] A typical maximum CA of a water droplet ranges from 110° to 115° on a flat entirely hydrophobic surface contacting air.[8,9] However, this limit may be far overtaken once proper roughness is introduced into the surface structures.[10] These super-hydrophobic and self-cleaning surfaces are widely used in various domains, such as drug delivery, micro-patterning, self-cleaning coatings, anti-reflection and oil removal.[11–14] Furthermore, surface composition and micro/nano topography are found as key factors to endow super-hydrophobicity.[15]

Among various superhydrophobic materials, coordination compounds distinguish themselves with unique biological activity and anti-cancer sterilization.[16,17] These compounds are also engineered and used in magnetics, photoluminescence, conductors, gas storage, catalysis, molecular recognition and isomer separation. Recently hybrid micro- or nano-composites utilizing natural leaves as raw materials have attracted keen interests to develop novel eco-friendly materials. Their unique properties enable the applications to selectively spilt/capture oil and work as high energy super-capacitors, *etc.*[18,19] In a coordination compound, a transition metal with lone pair electrons can act as the coordinate center. For example, there are various functional Zn(II) coordination compounds resulting due to the d^{10} electron structures of zinc. The Zn(II) coordination compounds have been used

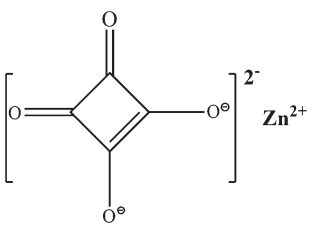

Scheme 1 Tentative molecular structure of ZnC_4O_4 with a squarate anion.

[a] *College of Chemistry, Key Lab of Environment Friendly Chemistry and Application in Ministry of Education, Xiangtan University, Xiangtan, China. E-mail: fengli_xtu@hotmail.com; Fax: +86 731 58292251; Tel: +86 731 58292206*
[b] *Nano and Molecular Systems Research Unit, Faculty of Science, University of Oulu, P. O. Box 3000, FIN-90014, Finland*
† The authors declare no competing financial interest.

as pesticides in agriculture, such as the fungicide Dithane (Parzate zineb) and mancozeb (Dithane M-45).[20] The Zn complexes are also widely used in medical research and luminescent materials.[21,22] The group of Zn coordination complexes may be simple in structures and compositions, but are important in functionalities. Robl successfully prepared ZnC_4O_4 (Scheme 1) crystals *via* aqueous gel chromatography in 1988.[23] However, there is no report on the lipo- or hydro-wettability of ZnC_4O_4, nor general, potential material applications. The synthesis routes were limited to the ones given by Robl, and facile routes such as the one-pot hydrothermal method have never been reported.

Herein, we present a one-pot hydrothermal route to fabricate ZnC_4O_4, which was employed to form super-hydrophobic surfaces after material self-assembly. The entire process to reach the desired material functionality is very simple, low-cost and environmentally friendly. Impacts of reaction time, surfactant and temperature on morphologies and super-hydrophobic properties of ZnC_4O_4 were well explored. The as-obtained ZnC_4O_4 had well-defined crystallographic facets and showed significant super-hydrophobic and superoleophilic properties. The crystal growth mechanism and origins leading to the wettability are also given.

Experimental

Preparation of ZnC_4O_4

All chemicals were analytical-grade reagents and used without further purification. A flow diagram of the sample preparation and modification steps is given in Scheme 2 for the ZnC_4O_4 with diverse morphologies. The synthesis route was as follows: 0.108 g squaric acid (H_2SA) and 0.42 g $Zn(OH)_2$ were added into 16 mL deionized water with vigorous stirring and then surfactants were added to the mixture. The mixture was agitated at 140 °C, 160 °C and 180 °C for 40 h. Cooling to room temperature in the air, the resulting solutions were centrifuged for 5 min at 4000 rpm to separate the solid powder products. The products were purified using ethanol. The effects of different surfactants (0.05 g EDTA-2Na, 0.05 g CTAB, 0.05 g PVP and 0.05 g citric acid), reaction temperature (140 °C, 160 °C and 180 °C) and reaction time (10 h, 20 h, 30 h and 40 h) on the morphological and structural properties of the samples were investigated.

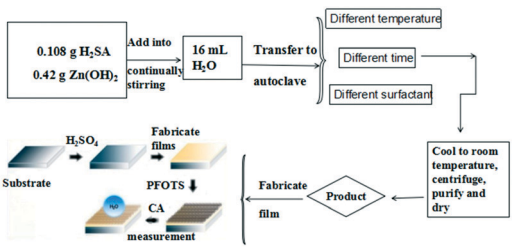

Scheme 2 Flow diagram of the sample preparation and modification steps.

Characterization

Product crystallizations were examined employing an X-ray powder diffractometer (XRD, MiniFlex II) using Cu Kα radiation (λ = 0.15406 nm) at 40 kV and 30 mA with a 0.04 (° s^{-1}) scanning rate in the 20–70° 2θ range. The powder samples were ultrasonically dispersed in ethanol and then deposited and dried on a holey carbon film on a copper grid. The scanning electronic microscopy (SEM) images were recorded on a JEOL JSM-6700F electron microscope and TEM, JEM-2100F, JEOL, Japan to detect the size of the products. The composition was determined through energy dispersive X-ray spectroscopy measurements (EDX, EX-250, Horiba, Japan). Chemical states of the elements in samples were deduced from the X-ray photoelectron spectroscopy (XPS, Escalab 250, Thermo Scientific, USA). The contact angles (CA) were measured by Ramé-hart Model p/n 250-F1.

Preparation of superhydrophobic surface

The surface of the glass substrate was cleaned using concentrated sulfuric acid to steep for 12 h and then continuously boiled for 2 h. After that, absolute ethanol and acetone were used alternately with ultrasound treatment three times to remove the organic pollutants, and then the surface was etched with 30% hydrochloric acid aqueous solution. The super-hydrophobic surface was prepared *via* a facile drop-casting method: first, a glass surface was modified *via* slow evaporation of a dilute ZnC_4O_4 ethanol dispersion, followed by drying at room temperature. In the second step, the films on a glass substrate were modified using methanol solution of 2% (v/v) PFOTS or 10 mmol L^{-1} stearic acid, and subsequently dried at 120 °C for 1 h.

Results and discussion

The chemical composition and crystal structure of the samples were determined *via* powder X-ray diffraction (XRD) measurements. Fig. 1a presents the XRD pattern of the as-synthesized product powder at 180 °C for 40 h without surfactant and the simulated pattern obtained using crystal data from a single crystal structure analysis. The peaks are strong and narrow, indicating good crystallinity of the as-prepared sample. The powder XRD pattern of ZnC_4O_4 is similar to the simulated pattern, as stated in ref. 23. The powder pattern

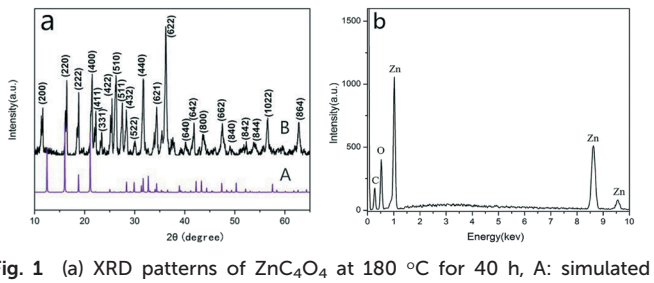

Fig. 1 (a) XRD patterns of ZnC_4O_4 at 180 °C for 40 h, A: simulated XRD pattern; B: XRD pattern of the as-synthesized product. (b) EDX spectrum of ZnC_4O_4 at 180 °C for 40 h.

shows a pure orthorhombic space group of ZnC_4O_4 with lattice constants of a = 9.012 Å, b = 13.336 Å, c = 6.746 Å, and the diffraction angle and intensity of the characteristic peaks of the samples are well consistent with ref. 23. Although XRD is able to verify the crystallized compounds in the products, amorphous components or impurities could not be figured out. We further carried out the elemental analysis using the as-synthesized product powder at 180 °C for 40 h. From Fig. 1b we could see that there was no other element except Zn, C and O, which proved that hydrothermal method is an efficient way to synthesis ZnC_4O_4: moreover it proved that the hydrothermal synthesis of complexes could improve the purity of the product.

To investigate the effect of reaction conditions on the ZnC_4O_4 formation, a series of comparative experiments was carried out through the similar process. The chemical composition and crystal structure of the samples were also determined *via* powder XRD measurements. The XRD patterns of ZnC_4O_4 samples prepared at different reaction temperatures (140 °C, 160 °C and 180 °C) for 40 h are presented in Fig. 2. As shown in Fig. 2, the XRD pattern of ZnC_4O_4 obtained at 140 °C and 180 °C are almost the same as that of ZnC_4O_4 obtained at 160 °C, which indicates that these three samples were almost the same. The peaks are strong and narrow, indicating good crystallinity of the as-prepared samples.

The morphologies of the samples were investigated *via* SEM. Fig. 3 shows the SEM images of the samples prepared at different temperatures for 40 h. The SEM images show concave spherical morphologies that strongly depend on the crystal structure of ZnC_4O_4. We observed that the samples exhibited a diameter of about 10 μm at 180 °C (Fig. 3a and b). Fig. 3a and b display low and high magnification SEM images of the ZnC_4O_4. When the reaction temperature was decreased to 160 °C, the average diameter was reduced to ~8 μm (Fig. 3c). As shown in Fig. 3d, the concave spherical structure was replaced by a lamellar structure. This indicates that the fall in temperature is detrimental to constitute concave spherical structure of ZnC_4O_4.

Fig. 4 shows the XRD patterns of ZnC_4O_4 samples prepared with reaction times of 10 h, 20 h, 30 h and 40 h at 180 °C. No other impurity phases were detected, which indicated the concave spherical structure of ZnC_4O_4. As shown in

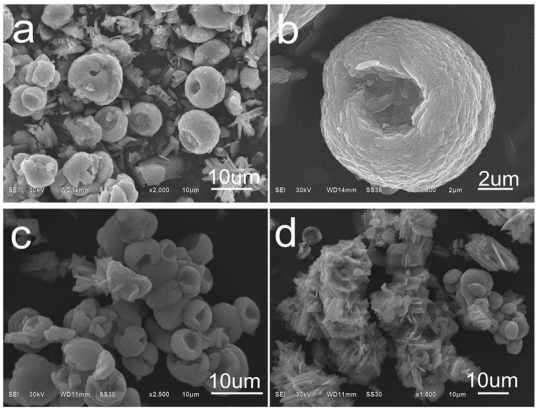

Fig. 3 SEM images for ZnC_4O_4 prepared at different reaction temperatures for 40 h (a) and (b) 180 °C, (c) 160 °C, and (d) 140 °C.

Fig. 4, the XRD pattern of ZnC_4O_4 obtained at 10 h is almost the same as that of ZnC_4O_4 obtained at 40 h, which indicates that these two samples were almost the same. The sharp diffraction peaks show that the products were well-crystallized. No characteristic peaks for impurities or other phases were observed. The products were pure ZnC_4O_4 in a single phase.

Fig. 5 shows the SEM images of ZnC_4O_4 samples prepared with reaction times of 10 h, 20 h, 30 h and 40 h at 180 °C. When the reaction time was 10 h, the crystals of the final product were irregular flakes (Fig. 5a). When the reaction time was longer than 20 h, a transition of ZnC_4O_4 from an irregular block structure to a regular circular block appeared. As the reaction time was increased to 40 h, the phase of ZnC_4O_4 turned into regular concave spherical completely (Fig. 5b–d). Thus, crystallinity, phase purity and morphological uniformity of products were considered to be highly correlative with the reaction time.

Surfactants can be adsorbed on the surfaces of the products effectively and control the growth of the products as the capping reagent. It has been reported that the selective adhesion of the capping ligand on the surface of crystals played an important role in the epitaxial growth of nanocrystals and microcrystals.[24–27] Therefore we investigated the important influence of surfactants on the shape of ZnC_4O_4 in our synthesis. The water ratio, quantity of reactants, reaction

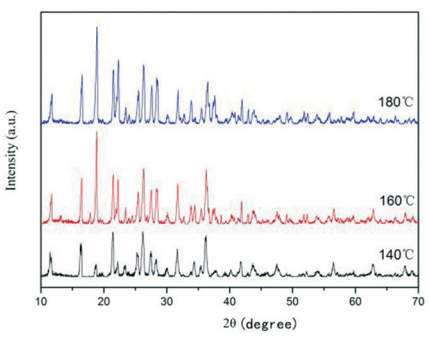

Fig. 2 XRD patterns of ZnC_4O_4 at different reaction temperatures for 40 h.

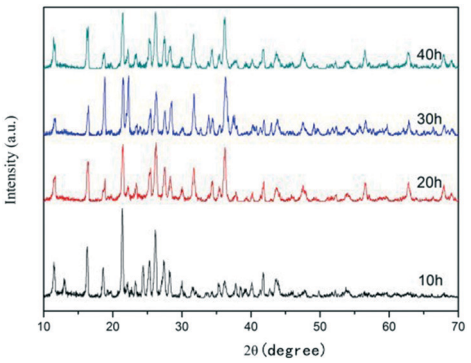

Fig. 4 XRD patterns of ZnC_4O_4 at different reaction times at 180 °C.

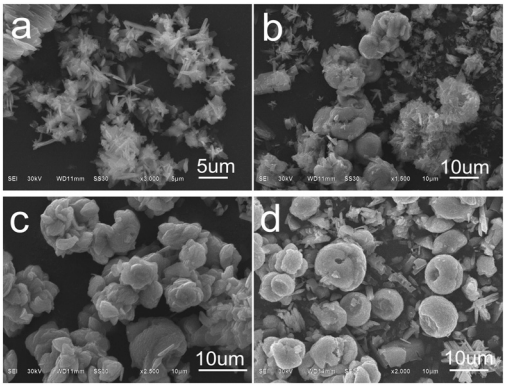

Fig. 5 SEM images for ZnC_4O_4 at different reaction times at 180 °C (a) 10 h, (b) 20 h, (c) 30 h, and (d) 40 h.

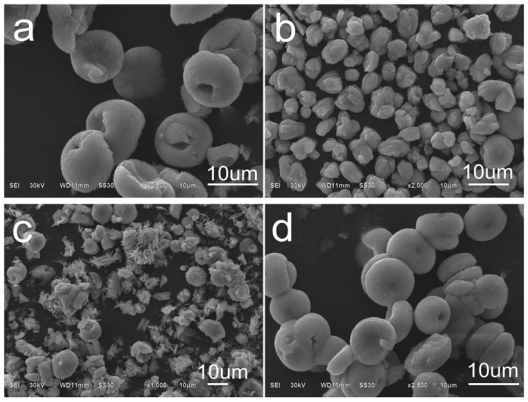

Fig. 7 SEM images for ZnC_4O_4 with different surfactants (180 °C and 40 h) (a) EDTA-2Na, (b) citric acid, (c) PVP and (d) CTAB.

temperature and time were kept constant (16 mL, 0.108 g H_4-BTCA, 0.42 g $Zn(OH)_2$, 180 °C and 40 h, respectively), and 0.05 g EDTA-2Na, 0.05 g citric acid, 0.05 g PVP and 0.05 g CTAB were selected as surfactants to investigate the effects on the shape of the ZnC_4O_4 crystals. Fig. 6 shows the XRD patterns of ZnC_4O_4 samples prepared with different surfactants. We can conclude from the Fig. 6a–d that the addition of surfactants did not affect the chemical composition and phase purity.

Fig. 7 shows the SEM patterns of ZnC_4O_4 samples (180 °C and 40 h). On adding EDTA-2Na and CTAB in the sample, there was little effect on the concave spherical product. Only the concave spherical surface became smoother and the recessed portion was reduced (Fig. 7a and d). When citric acid was introduced into the reaction system, a noticeable change in the crystals morphology was observed (Fig. 7b). The concave spherical product broke into discrete individual regular bulk crystals. With the addition of PVP, the product became a mixture of spherical and irregular bulk crystals. The as-obtained concave spherical structure could not be destroyed or broken into a discrete individual regular bulk crystal, which indicates that the microspheres were not a random aggregate of nanorods, but an ordered self-assembly.

More detailed structural information of the ZnC_4O_4 with different surfactants was further investigated *via* TEM and HRTEM. The TEM images in Fig. 8a and d show the morphology of the ZnC_4O_4 with EDTA-2Na and CTAB. From Fig. 8a and d, it can be seen that the blocks consisted of large-scale nanoplates with an average width of 10.93 μm and 8.81 μm. From the HRTEM images of Fig. 8b, c, e and f, for ZnC_4O_4 with EDTA-2Na and CTAB, it can be seen that the sample was entirely composed of a laminar structure with size about 10 nm and the lattice fringes with the spacing of d = 0.291 nm and 0.198 nm, corresponding to the (220) and (331) crystallographic planes of ZnC_4O_4, respectively.

X-ray photoelectron spectroscopy (XPS) was used to elucidate the surface compositions and chemical states of ZnC_4O_4 with different surfactants, namely, EDTA-2Na and CTAB materials. Fig. 9a is the survey scan XPS spectrum, which clearly indicates that the samples of the ZnC_4O_4 were mainly composed of Zn, C, and O elements. We can conclude from the Fig. 9a that there was no other prominent impurity peak of surfactants, and the surfactants did not affect the chemical composition and phase purity, which is consistent with the XRD results. In order to identify the chemical states of different elements, the XPS spectra of Zn 2p, C 1s and O 1s of the samples are presented in Fig. 9b–d, respectively. The Zn species of ZnC_4O_4 with different surfactants, namely, EDTA-2Na and CTAB displayed double peaks at both 1022.1 eV and

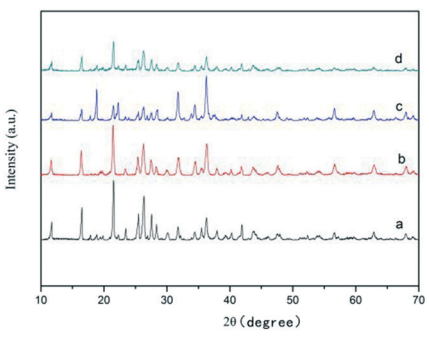

Fig. 6 XRD patterns of ZnC_4O_4 with different surfactants at 180 °C for 40 h (a) 0.05 g EDTA-2Na, (b) 0.05 g citric acid, (c) 0.05 g PVP and (d) 0.05 g CTAB.

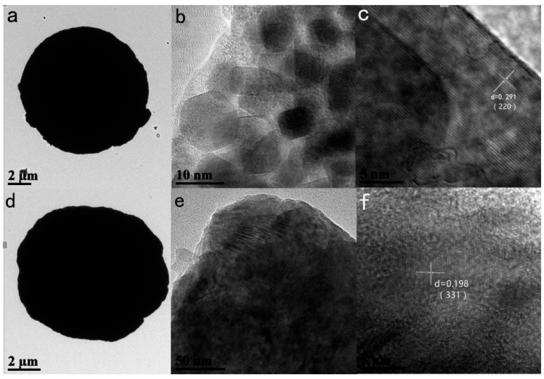

Fig. 8 (a–c) TEM and HRTEM images for ZnC_4O_4 with EDTA-2Na. (d–f) TEM and HRTEM images for ZnC_4O_4 with CTAB.

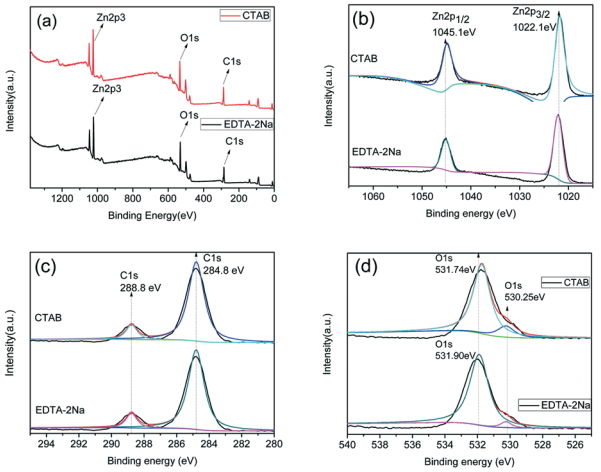

Fig. 9 XPS spectra of ZnC_4O_4 with different surfactants EDTA-2Na and CTAB (a) survey of the sample (b) Zn 2p (c) C1s (d) O1s.

1045.1 eV, referring to binding energies of Zn(II) 2p3/2 and Zn 2p1/2, respectively.[28] Fig. 9c shows the high-resolution XPS spectra of C 1s; the main peaks were found at approximately 284.8 eV and 288.8 eV, which can be attributed to the C–C bond with an sp^2 orbital and C=O bond with an sp orbital.[29] The O1s spectrum of the samples is shown in Fig. 9d, which can be fitted into two peaks at 530.25 eV and 531.90 eV in ZnC_4O_4 with EDTA-2Na surfactant and at 530.25 eV and 531.74 eV in ZnC_4O_4 with the surfactant of CTAB. The peak at 530.25 eV could be assigned to the coordination of oxygen in Zn–O, and the peak at 531.90 eV and 531.74 eV could be assigned to the C=O bond. The difference between the peaks of 531.90 eV and 531.74 eV could be attributed to the influence of the surfactants.

According to the abovementioned characterization, presumably, the formation of the ZnC_4O_4 concave spherical structure contained three important stages, namely, nucleation, crystal growth and self-assembly. Fig. 10 is a simulation diagram of the ZnC_4O_4 self-assembly growth process. First, the mixture of $Zn(OH)_2$ and $K_2C_4O_4$ solution formed ZnC_4O_4 amorphous particles, which are the precursor of crystal growth. Furthermore, after hydrothermal synthesis, small crystal particles gathered to generate nucleation, and with the reaction process, the direction of the crystal and crystallographic plane growth were different, leading to this type of laminated structure. Subsequently, driven by the electrostatic interactions, this laminated structure gathered slowly into a spherical construction. With the unceasing change of reaction temperature and other conditions, the concave spherical ZnC_4O_4 was finally obtained.

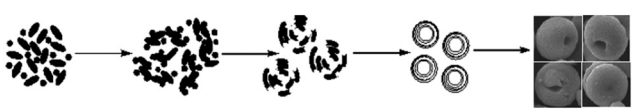

Fig. 10 Schematic of the proposed growth mechanism of ZnC_4O_4.

To simplify, one can envision a sorbent material with uniform, cylindrical pores. Based on such a model, it would be predicted that the ability of the liquid to be taken up by the porous material would critically depend on the contact angle value. According to Lucas Washburn equation, the rate and extent of liquid uptake are given as follows:

$$dL/dt = \gamma R \cos\theta/(4\eta L) \text{ or after solving for } L \quad (1)$$

$$L = [\gamma R t \cos\theta/(2\eta)]0.5 \quad (2)$$

where L is the liquid penetration distance after an elapsed time t, γ is the interfacial tension of the liquid, R the capillary radius (or an equivalent radius, when applying the model to noncylindrical pores), and θ is the contact angle (drawn through the liquid at the three-phase contact line). A key assumption of this simplified analysis is that no imbibition of liquid will occur if the contact angle exceeds 90 degrees. In fact, as noted before,[30] deviation from ideal smooth cylindrical pores tend to further inhibit passage of liquids through porous materials, even in cases where the contact angle on a corresponding smooth surface is less than 90 degrees.

Fig. 11a shows that the average CA of water droplets on the blank substrates was 64°, where the glass surface was not treated with any solution, which demonstrates the hydrophilic property of the substrate. Fig. 11b shows a 93° CA value of the water droplet where the glass surface was treated with a methanol solution of 2% (v/v) (PFOTS). After modifying with 2% (v/v) PFOTS, as shown in the Fig. 11c, the picture of water droplet on ZnC_4O_4 (180 °C, 40 h, without surfactant) surface indicated that the coating exhibited a superhydrophobic feature with a high 162° ± 0.5° static contact angle. We can see from the inset of Fig. 11d, that the CA values of the water droplet was 154° ± 0.5° where the glass surface was modified with a hexane solution of 10 mmol L^{-1} stearic acid. Moreover, Fig. 11e–f shows 151° ± 0.5° and 142° ± 0.5° CA values when a 5 wt% aqueous solution of NaCl was

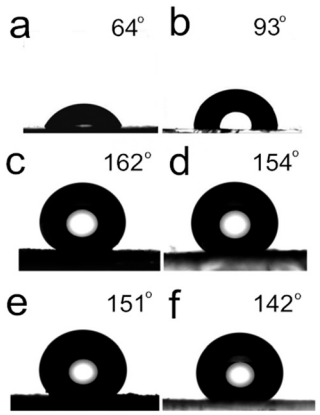

Fig. 11 Photographic images of the droplets of water (10 μL) on: (a) blank substrate, (b) the modified substrate with 2% (v/v) PFOTS, (c–d) surfaces of ZnC_4O_4 modifying with 2% (v/v) PFOTS and 10 mmol L^{-1} stearic acid; (e–f) the droplets of NaCl solution on modified ZnC_4O_4 surfaces with 2% (v/v) PFOTS and 10 mmol L^{-1} stearic acid.

dropped on the samples. The surface was modified with 2% (v/v) PFOTS and still reached the static CA of the super-hydrophobicity. It is assumed that the corrosion reaction of a 5 wt% aqueous solution of NaCl had little effect on the super-hydrophobic surface formed by ZnC_4O_4 samples. However, the surface that was modified with a hexane solution of 10 mmol L^{-1} stearic acid reached the static CA value for hydrophobicicity. These data can indicate that the surface modified with 2% (v/v) PFOTS was more stable than one modified with 10 mmol L^{-1} stearic acid.

Surface wettability of the as-synthesized ZnC_4O_4 (180 °C, 40 h, without surfactant) was studied *via* the measurement of the water CA using a water droplet (pH = 7) of 10 μL. It was observed that the wettability property of all the surfaces changed from hydrophilicity to super-hydrophobicity after the treatments with PFOTS. Without any chemical modification, the blank substrate surface showed hydrophilicity with a water contact angle less than 90°. However, after the simple chemical modification with PFOTS, the water droplet (pH = 7) contact angle of the ZnC_4O_4 increased to 162° ± 0.5°, which is the largest contact angle observed among all the different pH values (Fig. 12). In addition, the super-hydrophobicity of ZnC_4O_4 was studied *via* measuring the water CA using water droplets of 10 μL with different pH values. In contrast, the CA of products changed slightly on the changing pH value. When the pH values were 1, 3, 5, 7, 9, 11 and 13, the CA of products were 149.4° ± 0.5, 149° ± 0.5, 154° ± 0.5, 162° ± 0.5, 150.4° ± 0.5, 148.5° ± 0.5, and 143.5° ± 0.5, respectively. From the data analysis, it can be concluded that the as-prepared ZnC_4O_4 surfaces showed superhydrophobicity for some corrosive liquids, such as basic and acidic solutions.

Morphology is an important factor influencing the super hydrophobic performance. Based on previous experiments, reaction temperature plays a crucial role in the sample morphology. Thus, preparation temperature is a significant factor for the surfaces' hydrophobic performance. Fig. 13a, f and e show the surface contact angle of ZnC_4O_4 at 180 °C, 160 °C and 140 °C reaction temperatures (40 h). It could be observed that when the temperature was set as high as 180 °C and 160 °C, the static contact angle was 162° and 158.9°, above the super hydrophobic limit; however, it was only 145.2° when the temperature was 140 °C. The main reason for this is that the product at 180 °C and 160 °C was concave spherical, and only under 140 °C it showed a layered structure of small pieces. Concave spherical structure was beneficial to construct the super-hydrophobic structure. However the layered patch structure was adverse to hydrophobic structure, which affected its super hydrophobic properties. Similarly, time has influence on the products' morphology. Fig. 13a–d shows the static contact angle of the samples prepared at 180 °C with 40 h, 30 h, 20 h and 10 h reaction time. Through the figure, it is clear that the sample prepared at 40 h has the highest static CA, followed by the one at 30 h. Four groups of data show that under 180 °C at different reaction times, all the ZnC_4O_4 products had super hydrophobic properties, and the hydrophobic effect increased with increasing reaction time.

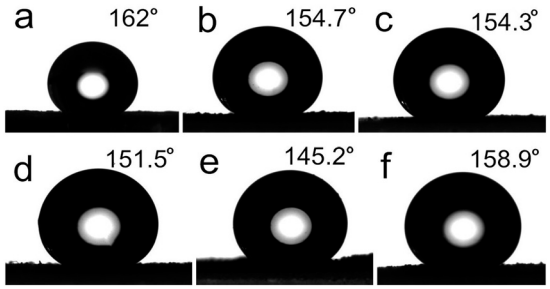

Fig. 13 Impact of temperature and time on the ZnC_4O_4 super hydrophobic surface (a) 180 °C, 40 h; (b) 180 °C, 30 h; (c) 180 °C, 20 h; (d) 180 °C, 10 h; (e) 140 °C, 40 h; (f) 160 °C, 40 h.

Fig. 14a–d show the surface CAs of ZnC_4O_4 modified with surfactants after treatments with PFOTS. Values of 152.7°, 154.1°, 152.9° and 153.4° were determined after adding EDTA-2Na, HLC, PVP and CTAB, respectively. In TEM images, the ZnC_4O_4 morphology had no evident change with EDTA-2Na and CTAB surfactants and still kept the original concave spherical structure except concave part decreased, resulting in smaller CAs. This is perhaps because reducing the concave part cut down the interstice, and the resistance of the air decreased when the water droplet came in contact with the ZnC_4O_4 surface. Although the addition of these surfactants

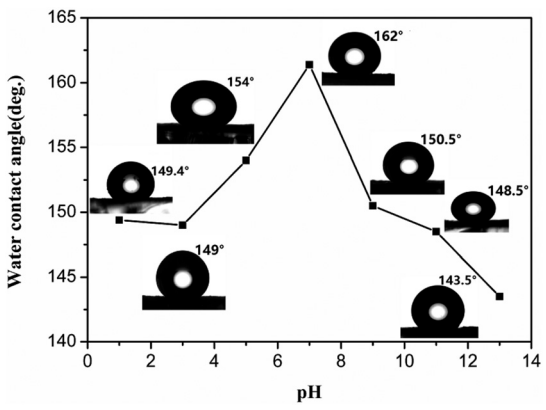

Fig. 12 Water contact angles of the modified resulting surface according to the pH of water droplet.

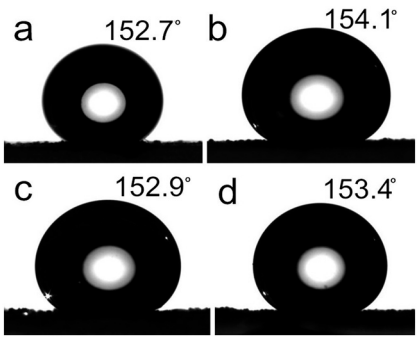

Fig. 14 The static contact angle of ZnC_4O_4 surface added different surfactants. (a) EDTA-2Na, (b) HLC, (c) PVP, (d) CTAB.

influenced the static contact angle of the ZnC_4O_4 ultra thin surface, the ZnC_4O_4 surface could still achieve super hydrophobic properties. Fig. 15 shows the SEM images of ZnC_4O_4 films before and after being modified by PFOTS, with their corresponding magnified images depicted as insets. It was found that the surface free energy of ZnC_4O_4 rough structure was reduced by low surface energy groups of $-CF_2$ and $-CF_3$ from the PFOTS. As a consequence, a large amount of spherical agglomeration appeared on the surface uniformly, resulting in bigger contact angles on the PFOTS-modified ZnC_4O_4 film.

The morphology of solid surface is a considerable factor for the wettability of the as-prepared product. Fig. 16 shows the surface morphology of different ZnC_4O_4 films without PFOTS modification, and the inserted pictures are the corresponding magnified images. From the figure, it can be concluded that the drop-casting method does not change the original appearance of the as-prepared sample. The surface of the ZnC_4O_4 films possessed structures with extended roughness and complex characteristics, which was consistent with the as-prepared sample. There was no aggregation in the ZnC_4O_4 films, and the sample could disperse uniformly with a porous network. Films of ZnC_4O_4 with different surfactants are shown in Fig. 16a (EDTA-2Na) and b (PVP). Morphologies of the solid surfaces were almost identical, resulting in almost the same contact angles of 152.7° and 152.9°. Fig. 16c and d show SEM images of films casted with ZnC_4O_4 prepared at different reaction times of 40 h and 20 h, respectively. It can be seen that more regular concave spherical phases of ZnC_4O_4 were dispersed onto solid surfaces following the reaction time. These spheres bring higher contact angles of the ZnC_4O_4 films (see the abovementioned analysis of contact angle for ZnC_4O_4 films).

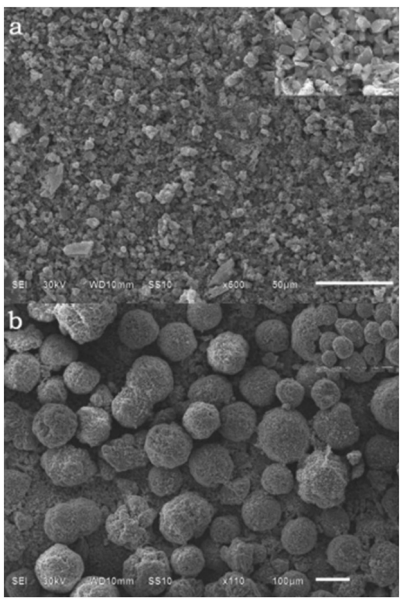

Fig. 15 SEM images of different ZnC_4O_4 films (a) before and (b) after modification using PFOTS.

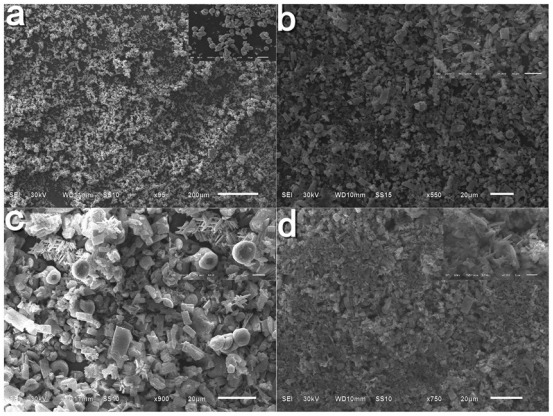

Fig. 16 SEM images for different ZnC_4O_4 films (a) 180 °C, 40 h, EDTA-2Na (b) 180 °C, 40 h, PVP, (c) 180 °C, 40 h, without surfactant and (d) 180 °C, 20 h, without surfactant.

The water adhesion, which is an important property of a solid surface, can be accurately assessed *via* the sliding behavior of a water droplet. We carried out a rolling test of water droplets. When the sample was tilted a little, the water droplet rolled off freely on the front part of the surface like that of a water droplet on a lotus leaf. As shown in Fig. 17, the water sliding angle on the surface was less than 5°. In such circumstances, the water droplet rolls rapidly when it is dropped onto the super hydrophobic surface and the water droplets rarely stick to it. This phenomenon may be utilized for solid transfer and control of droplet movement.

In order to study the surface morphology and surface chemical modifying effect on the properties of the superhydrophobic surface, and based on the previous work, the mechanism of the ZnC_4O_4 super-hydrophobic surfaces were discussed as follows. The super-hydrophobic surface was covered by fluoroalkylsilane, which greatly reduced the free energy of the surface. The abovementioned films post-grafted with fluoroalkyl, may through covalent linkage of Si–O/C–O and a modifying molecule, link to each other by Si–O–Si bonds.[31,32] The super-hydrophobic surfaces composed of concave spherical structures trapped a large amount of air within them and formed the Cassie state. Water droplets were prevented by the gas layer trapped in the microscales.[33]

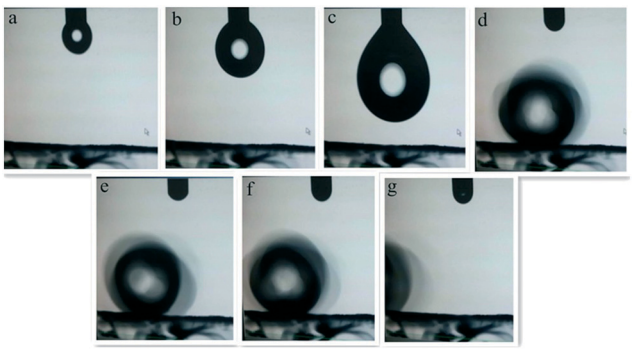

Fig. 17 Video snapshots of a sliding water droplet on the surface of the ZnC_4O_4 sample (a–g): rolling conditions of the drop with temporal variation.

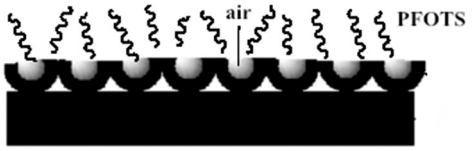

Fig. 18 Formation of the self-assembled ZnC_4O_4 super-hydrophobic surface.

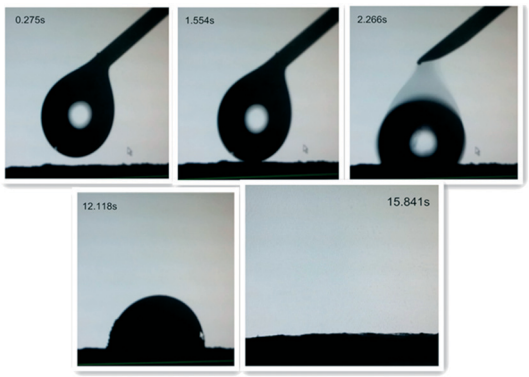

Fig. 19 Video snapshots of a drop of octane absorbed by the as-prepared ZnC_4O_4 sample with doping.

PFOTS contained low surface energy with $-CF_3$ and $-CF_2$ groups, which could reduce the free energy of the ZnC_4O_4 rough structures. The self-assembly process of PFOTS on the ZnC_4O_4 surfaces is shown in Fig. 18. First, the reaction of silicon ethoxide ($Si-OC_2H_5$) functional groups with water formed silanol (Si–OH), which acted as the reactive group at the end of the molecule. The silanol reacted with –OH groups to subsequently form a self-assembled film, and polysiloxane was grafted onto the surface by inducing vertical polymerization.[34]

Contact angle measurements revealed that the as-prepared ZnC_4O_4 surface displayed superoleophilic properties. Video snapshots of a drop of octane absorbed by the as-prepared ZnC_4O_4 surface is shown in Fig. 19. The time taken to absorb a drop of octane by the as-prepared surface was 15.841 s, which shows that the as-prepared ZnC_4O_4 samples absorbed oil quickly, but repelled water completely.

Conclusion

In summary, a series of ZnC_4O_4 micro crystals were prepared *via* a simple hydrothermal synthesis procedure at different reaction conditions. The reaction temperature, reaction time, as well as the different surfactants, playing a very important role in the growth process of concave spherical ZnC_4O_4 have been discussed. The results showed that the materials presented long-term stability in air as well as excellent resistance to corrosive liquids, including alkaline, weakly acidic and salt solutions. The present study provides a new strategy to prepare novel functional materials with potential industrial applications, such as self-cleaning, corrosion prevention and oil/water separation.

Acknowledgements

The authors acknowledge with thanks the financial support of the Provincial Natural Science Foundation of Hunan, China (2015JJ2138), the National Natural Science Foundation of China (21601149), and the Strategic Grant from University of Oulu, Finland, and the European Union Regional Development Foundation.

Notes and references

1 K. Koch and W. Barthlott, *Philos. Trans. R. Soc., A*, 2009, **367**, 1487.
2 K. Jin, J. C. Cremaldi, J. S. Erickson, Y. Tian, J. N. Israelachvili and N. S. Pesika, *Adv. Funct. Mater.*, 2014, **24**, 574–579.
3 A. Irzh, L. Ghindes and A. Gedanken, *ACS Appl. Mater. Interfaces*, 2011, **3**, 4566–4572.
4 M. Callies and D. Quéré, *Soft Matter*, 2005, **1**, 55–61.
5 X. J. Feng and L. Jiang, *Adv. Mater.*, 2006, **18**, 3063–3078.
6 X. M. Li, D. Reinhoudt and M. Crego-Calama, *Chem. Soc. Rev.*, 2007, **36**, 1350–1368.
7 A. B. D. Cassie and S. Baxter, *Trans. Faraday Soc.*, 1944, **40**, 546–551.
8 N. Tillman, A. Ulman and T. L. Penner, *Langmuir*, 1989, **5**(1), 101–111.
9 M. K. Chaudhury, *J. Adhes. Sci. Technol.*, 1996, **7**(6), 669–675.
10 S. Wang and L. Jiang, *Adv. Mater.*, 2007, **19**, 3423.
11 S. Nagappan, S. S. Park and C. S. Ha, *J. Nanosci. Nanotechnol.*, 2014, **14**, 1441–1462.
12 E. Celia, T. Darmanin, E. T. Givenchy, S. Amigoni and F. Guittard, *J. Colloid Interface Sci.*, 2013, **402**, 1.
13 F. L. Geyer, E. Ueda, U. Liebel, N. Grau and P. A. Levkin, *Angew. Chem., Int. Ed.*, 2011, **50**, 8424.
14 B. J. Basu and J. Manasa, *Appl. Phys. A: Mater. Sci. Process.*, 2011, **103**, 343.
15 X. Zhang, F. Shi, J. Niu, Y. G. Jiang and Z. Q. Wang, *J. Mater. Chem.*, 2008, **18**, 621.
16 S. Odisitse, G. E. Jackson and T. Govender, *Dalton Trans.*, 2007, 140.
17 P. Gautam, N. Sharma, K. Chaturvedi and G. K. Chaturvedi, *J. Indian Chem. Soc.*, 2006, **83**, 269.
18 S. Nagappan, J. J. Park, S. S. Park, W. K. Lee and C. S. Ha, *J. Mater. Chem. A*, 2013, **1**, 6761.
19 M. Biswal, A. Banerjee, M. Deo and S. Ogale, *Energy Environ. Sci.*, 2013, **6**, 1249.
20 L. Mishra, A. Jha and A. K. Yadaw, *Transit. Met. Chem.*, 1997, **22**, 406–410.
21 F. A. Monhaned, S. A. Aay and H. M. Abdel-Rahman, *Bull. Pharm. Sci.*, 2003, **26**, 187.
22 E. C. Yang, H. K. Zhao, B. Ding, X. G. Wang and X. J. Zhao, *Cryst. Growth Des.*, 2007, **7**, 2009.

23 C. Robl and W. F. Kuhs, *J. Solid State Chem.*, 1988, **75**, 15–20.
24 X. G. Peng, L. Manna, W. D. Yang, J. Wickham, E. Scher, A. Kadabanich and A. P. Alivisatos, *Nature*, 2000, **404**, 59.
25 T. Xie, S. Li, W. B. Wang, Q. Peng and Y. D. Li, *Chem. – Eur. J.*, 2008, **14**, 9730.
26 X. M. Sun and Y. D. Li, *Adv. Mater.*, 2005, **17**, 2626.
27 R. Si, Y. W. Zhang, L. P. You and C. H. Yan, *Angew. Chem., Int. Ed.*, 2005, **44**, 3256.
28 M. S. Killian, J. F. Gnichwitz, A. Hirsch, P. Schmuki and J. Kunze, *Langmuir*, 2010, **26**, 3531.
29 B. F. Luo, D. B. Xu, D. Li, G. L. Wu, M. M. Wu, W. D. Shi and M. Chen, *ACS Appl. Mater. Interfaces*, 2015, **7**, 17061–17069.
30 H. J. Kent and M. B. Lyne, *Nord. Pulp Pap. Res. J.*, 1989, **4**, 141.
31 T. Pisuchpen, N. Chaim-ngoen, N. Intasanta, P. Supaphol and V. P. Hoven, *Langmuir*, 2011, **27**, 3654.
32 N. M. Oliveira, R. L. Reis and J. F. Mano, *ACS Appl. Mater. Interfaces*, 2013, **5**, 4202.
33 J. Ou, W. Hu, C. Li, Y. Wang, M. Xue, F. Wang and W. Li, *ACS Appl. Mater. Interfaces*, 2012, **4**, 5737.
34 W. J. Xu, J. L. Song, J. Sun, Y. Lu and Z. Y. Yu, *ACS Appl. Mater. Interfaces*, 2011, **3**, 4404.

